

Electronic Supplementary Information (ESI)

Facile dimerization strategy for producing narrowband green multi-resonance delayed fluorescence emitters

Minlang Yang, Rajendra Kumar Konidena, So Shikita and Takuma Yasuda*

Institute for Advanced Study and Department of Applied Chemistry, Graduate School of Engineering, Kyushu University

744 Motoooka, Nishi-ku, Fukuoka 819-0395, Japan

E-mail: yasuda@ifrc.kyushu-u.ac.jp

Table of Contents:

| | |
|--------------------------------------------------------------------------------------|---------|
| 1. General Methods | S2 |
| 2. Computational Simulations | S2 |
| 3. Photophysical Measurements | S3 |
| 4. OLED Fabrication and Evaluation | S3 |
| 5. Synthesis and Characterization | S4–S5 |
| Fig. S1 ¹ H and ¹³ C NMR spectra of <i>p</i> -CzB | S6 |
| Fig. S2 ¹ H and ¹³ C NMR spectra of <i>m</i> -CzB | S7 |
| Fig. S3 X-ray structure of <i>m</i> -CzB | S8 |
| Fig. S4 TGA thermograms | S8 |
| Fig. S5 PL data of the doped films with doping different concentration | S9 |
| Fig. S6 Fluorescence and phosphorescence spectra | S9 |
| Fig. S7 Transient PL decay curves in solutions | S10 |
| Fig. S8 Temperature dependence of transient PL decay curves | S10 |
| Fig. S9 Comparison of k_{RISC} for green MR-TADF emitters | S10 |
| Fig. S10 OLED device structure and materials | S11 |
| Fig. S11 Operational stability tests for OLEDs | S11 |
| Table S1 PL and EL data for green MR-TADF emitters | S12 |
| References | S13–S14 |

1. General Methods

All reagents and anhydrous solvents were purchased from Sigma-Aldrich, Tokyo Chemical Industry (TCI), or Fujifilm Wako Pure Chemical Corp., and were used without further purification unless otherwise noted. 1,3-bis(1,8-dimethylcarbazol-9-yl)benzene (mMCP),^[S1] 3,3'-di(carbazol-9-yl)-5-cyano-1,1'-biphenyl (mCBP-CN),^[S2] and 1,3-bis[3,5-di(pyridin-3-yl)phenyl]benzene (B3PyPB)^[S3] were prepared according to the literature procedures and purified by vacuum sublimation before use. 2,8-Bis(diphenylphosphinyl)dibenzo[b,d]furan (PPF) was purchased from TCI and purified by vacuum sublimation before use. 2,3,6,7,10,11-Hexacyano-1,4,5,8,9,12-hexaazatriphenylene (HAT-CN), 1,1-bis[4-[*N,N*-di(*p*-tolyl)amino]phenyl]cyclohexane (TAPC), and 8-quinolinolato lithium (Liq) were purchased from LG Chem Ltd., Luminescence Technology Corp., and e-Ray Optoelectronics Technology Co., Ltd., respectively, and used as received.

NMR spectra were recorded on an Avance III 400 spectrometer (Bruker). ¹H and ¹³C NMR chemical shifts were determined relative to the signals of tetramethylsilane ($\delta = 0.00$) and CDCl₃ ($\delta = 77.0$), respectively. Matrix-assisted laser desorption ionization time-of-flight (MALDI-TOF) mass spectra were collected on an Autoflex III spectrometer (Bruker Daltonics) using dithranol as a matrix. Elemental analysis was carried out using an MT-5 CHN corder (Yanaco). Vacuum sublimation was performed using a P-100 system (ALS Technology). Thermogravimetric analysis (TGA) was performed on a TG/DTA7300 analyzer (Hitachi High-Tech Science) under a N₂ atmosphere.

2. Computational Simulations

All quantum chemical calculations based on the time-dependent density functional theory (TD-DFT) were performed using the ADF2021 program package.^[S4] The ground-state (S_0) geometries were initially optimized using the B3LYP functional with the DZP basis set in the gas phase. The vertical excitation calculations were carried out using the optimized S_0 geometries, and the geometry optimizations in the excited S_m ($m = 1, 2$) and T_n ($n = 1-4$) states were performed using TD-DFT at the same level of theory. For the $S_0 \rightarrow S_m$ and $S_0 \rightarrow T_n$ transitions, the natural transition orbitals (NTOs) with their adiabatic excitation energies were simulated using the optimized S_m and T_n geometries, respectively. Using the respective T_n geometries, spin-orbit coupling (SOC) matrix elements, $\langle S_m | \hat{H}_{\text{SOC}} | T_n \rangle$, were calculated using a scalar relativistic TD-DFT with the two-component zeroth-order relativistic approximation (ZORA)^[S5] at the same level of theory. The contributions of the three degenerate triplet states ($T_{n,x}$, $T_{n,y}$, and $T_{n,z}$) were taken into account by calculating the root sum square of the real (Re) and imaginary (Im) parts of the matrix elements, as expressed by the following equation:^[S6]

$$\langle S_m | \hat{H}_{\text{SOC}} | T_n \rangle = \left\{ \sum_{a=x,y,z} (\text{Re}^2 \langle S_m | \hat{H}_{\text{SOC}} | T_{n,a} \rangle + \text{Im}^2 \langle S_m | \hat{H}_{\text{SOC}} | T_{n,a} \rangle) \right\}^{1/2} \quad (\text{Eq. S1})$$

3. Photophysical Measurements

Organic thin-film samples for photophysical measurements were deposited onto quartz substrates via vacuum deposition ($< 7 \times 10^{-5}$ Pa) using an E-200 vacuum evaporation system (ALS Technology). UV-vis absorption and photoluminescence (PL) spectra were measured using a V-670Y spectrometer (Jasco) and an FP-8600Y spectrophotometer (Jasco), respectively. The absolute PL quantum yields (Φ_{PL}) were determined using an ILF-835 integrating sphere system (Jasco) under a N_2 atmosphere. Transient PL decay measurements were carried out using a C11367 Quantaaurus-tau fluorescence lifetime spectrometer (Hamamatsu Photonics) with an LED excitation source ($\lambda_{\text{ex}} = 340$ nm, pulse width = 100 ps, repetition rate = 1 kHz) under a N_2 atmosphere. The emission lifetimes were determined from the PL decay curves by performing exponential fitting and deconvolution with the instrument response function.

The photophysical rate constants for radiative decay (k_{r}), non-radiative decay (k_{nr}), intersystem crossing (k_{ISC}), and reverse intersystem crossing (k_{RISC}) were calculated according to the literature method:^[S7] $k_{\text{r}} = \Phi_{\text{p}}/\tau_{\text{p}}$; $k_{\text{ISC}} = (1 - \Phi_{\text{p}})/\tau_{\text{p}}$; $k_{\text{RISC}} = \Phi_{\text{d}} \cdot (k_{\text{ISC}} \cdot \tau_{\text{p}} \cdot \tau_{\text{d}} \cdot \Phi_{\text{p}})$, where Φ_{p} and Φ_{d} are fractional quantum yields for prompt fluorescence and delayed fluorescence, and τ_{p} and τ_{d} are emission lifetimes for prompt fluorescence and delayed fluorescence, respectively.

4. OLED Fabrication and Evaluation

Indium-tin-oxide (ITO)-coated glass substrates were cleaned with detergent, deionized water, acetone, and isopropanol in this order. The substrates were then subjected to UV-ozone treatment for 30 min before loading into an E-200 vacuum evaporation system (ALS Technology). Organic layers and a cathode aluminum layer were thermally evaporated on the substrates under vacuum ($< 6 \times 10^{-5}$ Pa) with a deposition rate of < 0.3 nm s^{-1} through a shadow mask, defining a pixel size of 0.04 cm². The layer thickness and deposition rate were monitored *in situ* during deposition by oscillating quartz thickness monitors. The J - V - L characteristics of the fabricated OLEDs were measured using a 2400 source meter (Keithley) and a CS-2000 spectroradiometer (Konica Minolta). The EL efficiencies were corrected by the Lambertian factors evaluated from the angle-resolved EL data. The device lifetime tests were performed using an EAS-31D OLED lifetime evaluation system (System Engineers). The luminance of each test device was measured under the constant current driving conditions with an initial luminance of 100 cd m^{-2} .

5. Synthesis and Characterization

All chemical reactions were performed under a dry N₂ atmosphere using anhydrous solvents unless otherwise noted.

Synthesis of 1: 3,6-Di-*tert*-butylcarbazole (13.97 g, 50.0 mmol) and *t*-BuOK (5.61 g, 50.0 mmol) were dissolved in DMF (200 mL) at room temperature. After stirring for 30 min, 5-bromo-1,3-difluoro-2-iodobenzene (6.38 g, 20.0 mmol) was added to the solution. The mixture was stirred at 100 °C for 12 h. After cooling to room temperature, the reaction mixture was added into a large amount of water and then extracted with CH₂Cl₂. The combined organic layer was washed with water and dried over anhydrous Na₂SO₄. After filtration and evaporation, the crude product was purified by silica gel column chromatography (eluent: hexane/CH₂Cl₂ = 4:1, v/v), followed by recrystallization from CH₂Cl₂/methanol to afford **1** as a white solid (yield = 12.57 g, 75%). ¹H NMR (400 MHz, CDCl₃): δ 8.16 (s, 4H), 7.67 (s, 2H), 7.52 (d, *J* = 8.5 Hz, 4H), 7.11 (d, *J* = 8.5 Hz, 4H), 1.47 (s, 18H). ¹³C NMR (100 MHz, CDCl₃): δ 144.70, 143.45, 138.94, 133.37, 123.93, 123.55, 123.24, 116.57, 109.49, 104.14, 34.81, 32.03. MS (MALDI-TOF): *m/z* calcd 836.22 [*M*]⁺; found 836.43.

Synthesis of 2: To a solution of **1** (5.03 g, 6.0 mmol) in dry *t*-butylbenzene (120 mL) was slowly added *n*-BuLi (1.6 M in hexane, 4.1 mL, 6.6 mmol) at 0 °C. After reacting for 3 h at room temperature, BBr₃ (2.25 g, 9.0 mmol) was slowly added at 0 °C, and then the mixture was stirred at room temperature for 3 h. After addition of NEt(*i*-Pr)₂ (2.4 mL, 13.5 mmol) at 0 °C, the reaction mixture was further stirred at 160 °C for 24 h. After cooling to room temperature, the reaction mixture was carefully quenched by addition of water, and then extracted with toluene. The combined organic layer was dried over anhydrous Na₂SO₄. After filtration and evaporation, the crude product was purified by silica gel column chromatography (eluent: hexane/CH₂Cl₂ = 9:1, v/v), followed by recrystallization from CH₂Cl₂/methanol to afford **2** as a yellow solid (yield = 1.32 g, 31%). ¹H NMR (400 MHz, CDCl₃): δ 9.00 (s, 2H), 8.37 (s, 2H), 8.20 (s, 2H), 8.16-8.12 (m, 4H), 7.60 (d, *J* = 8.8 Hz, 2H), 1.66 (s, 18H), 1.52 (s, 18H). ¹³C NMR (100 MHz, CDCl₃): δ 145.63, 144.88, 144.54, 141.36, 137.94, 129.70, 127.66, 127.12, 124.45, 123.67, 121.52, 120.87, 120.77, 117.22, 114.00, 110.77, 35.18, 34.80, 32.17, 31.81. MS (MALDI-TOF): *m/z* calcd 718.31 [*M*]⁺; found 718.38.

Synthesis of 3: A mixture of **2** (0.72 g, 1.0 mmol), bis(pinacolato)diboron (0.38 g, 1.5 mmol), PdCl₂(dppf) (0.04 g, 0.05 mmol), and potassium acetate (0.29 g, 3.0 mmol) in dry 1,4-dioxane (15 mL) was stirred at 100 °C for 24 h. After cooling to room temperature, the reaction mixture was added into a large amount of water and then extracted with CH₂Cl₂. The combined organic layer was dried over anhydrous Na₂SO₄. After filtration and evaporation, the crude product was purified by silica gel column chromatography (eluent: hexane/CH₂Cl₂ = 2:1, v/v), followed by recrystallization from CH₂Cl₂/methanol to afford **3** as a yellow solid

(yield = 0.51 g, 67%) ^1H NMR (400 MHz, CDCl_3): δ 9.14 (s, 2H), 8.79 (s, 2H), 8.53 (d, J = 8.8 Hz, 2H), 8.48 (s, 2H), 8.27 (s, 2H), 7.74 (d, J = 8.5 Hz, 2H), 1.67 (s, 18H), 1.54 (s, 18H), 1.50 (s, 12H). ^{13}C NMR (100 MHz, CDCl_3): δ 145.18, 144.56, 143.69, 141.65, 138.51, 129.78, 126.97, 125.17, 124.56, 123.77, 121.68, 120.70, 119.07, 117.08, 114.45, 113.77, 84.35, 35.18, 34.82, 32.22, 31.87, 25.09. MS (MALDI-TOF): m/z calcd 766.48 [M] $^+$; found 766.64.

Synthesis of *p*-CzB: A mixture of **2** (0.36 g, 0.5 mmol), **3** (0.38 g, 0.5 mmol), $\text{Pd}(\text{PPh}_3)_4$ (0.008 g, 0.005 mmol), and Na_2CO_3 (0.21 g, 2.0 mmol) in toluene (14 mL), ethanol (4 mL), and water (2 mL) was stirred at 85 °C for 48 h. After cooling to room temperature, the reaction mixture was added into a large amount of water and then extracted with CH_2Cl_2 . The combined organic layer was dried over anhydrous Na_2SO_4 . After filtration and evaporation, the crude product was purified by silica gel column chromatography (eluent: hexane/ CH_2Cl_2 = 4:1, v/v), followed by recrystallization from CH_2Cl_2 /methanol to afford ***p*-CzB** as an orange solid (yield = 0.36 g, 56%). ^1H NMR (400 MHz, CDCl_3): δ 9.09 (s, 4H), 8.95 (s, 4H), 8.67 (d, J = 8.8 Hz, 4H), 8.45 (s, 4H), 8.25 (s, 4H), 7.63 (d, J = 8.8 Hz, 4H), 1.71 (s, 36H), 1.51 (s, 36H). ^{13}C NMR (100 MHz, CDCl_3): δ 146.06, 145.40, 144.99, 144.71, 141.82, 138.43, 129.87, 127.33, 124.35, 123.70, 122.85, 121.80, 120.61, 117.41, 114.28, 107.41, 35.21, 34.77, 32.25, 31.87. MS (MALDI-TOF): m/z calcd 1278.78 [M] $^+$; found 1278.87. Anal. calcd (%) for $\text{C}_{92}\text{H}_{96}\text{B}_2\text{N}_4$: C 86.37, H 7.56, N 4.38; found: C 86.11, H 7.56 N 4.29.

Synthesis of *m*-CzB: To a solution of **BBCz-SB**^[S8] (1.41 g, 2.2 mmol) in CH_2Cl_2 (88 mL) was slowly added $\text{Cu}(\text{ClO}_4)_2 \cdot 6\text{H}_2\text{O}$ (0.075 M in CH_3CN , 44 mL, 3.3 mmol) at room temperature. The mixture was stirred for 5 h at room temperature. After quenching by the addition of aqueous K_2CO_3 (3.3 M, 4.0 mL), the product was extracted with CHCl_3 . The combined organic layer was washed with water and dried over anhydrous Na_2SO_4 . After filtration and evaporation, the crude product was purified by silica gel column chromatography (eluent: hexane/ CHCl_3 = 1:1, v/v), preparative gel permeation chromatography (eluent: CHCl_3), followed by recrystallization from CHCl_3 /methanol to afford ***m*-CzB** as an orange solid (yield = 0.75 g, 54%). ^1H NMR (400 MHz, CDCl_3): δ 8.94 (d, J = 1.8 Hz, 2H), 8.76 (m, 4H), 8.72 (d, J = 1.8 Hz, 2H), 8.57 (d, J = 8.8 Hz, 2H), 8.44 (d, J = 1.8 Hz, 2H), 8.31 (d, J = 2.0 Hz, 2H), 7.75 (dd, J = 8.8, 2.0 Hz, 2H), 7.73 (d, J = 1.8 Hz, 2H), 7.09 (d, J = 1.5 Hz, 2H), 6.03 (d, J = 8.8 Hz, 2H), 5.97 (dd, J = 8.8, 2.0 Hz, 2H), 1.73 (s, 18H), 1.65 (s, 18H), 1.58 (s, 18H), 0.78 (s, 18H). ^{13}C NMR (100 MHz, CDCl_3): δ 145.24, 144.35, 143.52, 143.41, 142.98, 142.27, 141.22, 140.56, 138.26, 137.07, 135.67, 130.45, 128.64, 127.23, 126.42, 125.71, 124.25, 124.06, 123.26, 121.75, 120.73, 120.17, 119.28, 117.36, 115.41, 113.88, 111.48, 110.60, 35.15, 35.08, 34.87, 33.93, 32.46, 32.22, 31.91, 31.22 (Two aromatic signals could not be observed probably because of the overlapping). MS (MALDI-TOF): m/z calcd 1278.78 [M] $^+$; found 1278.72. Anal. calcd (%) for $\text{C}_{92}\text{H}_{96}\text{B}_2\text{N}_4$: C 86.37, H 7.56, N 4.38; found: C 86.43, H 7.60 N 4.35.

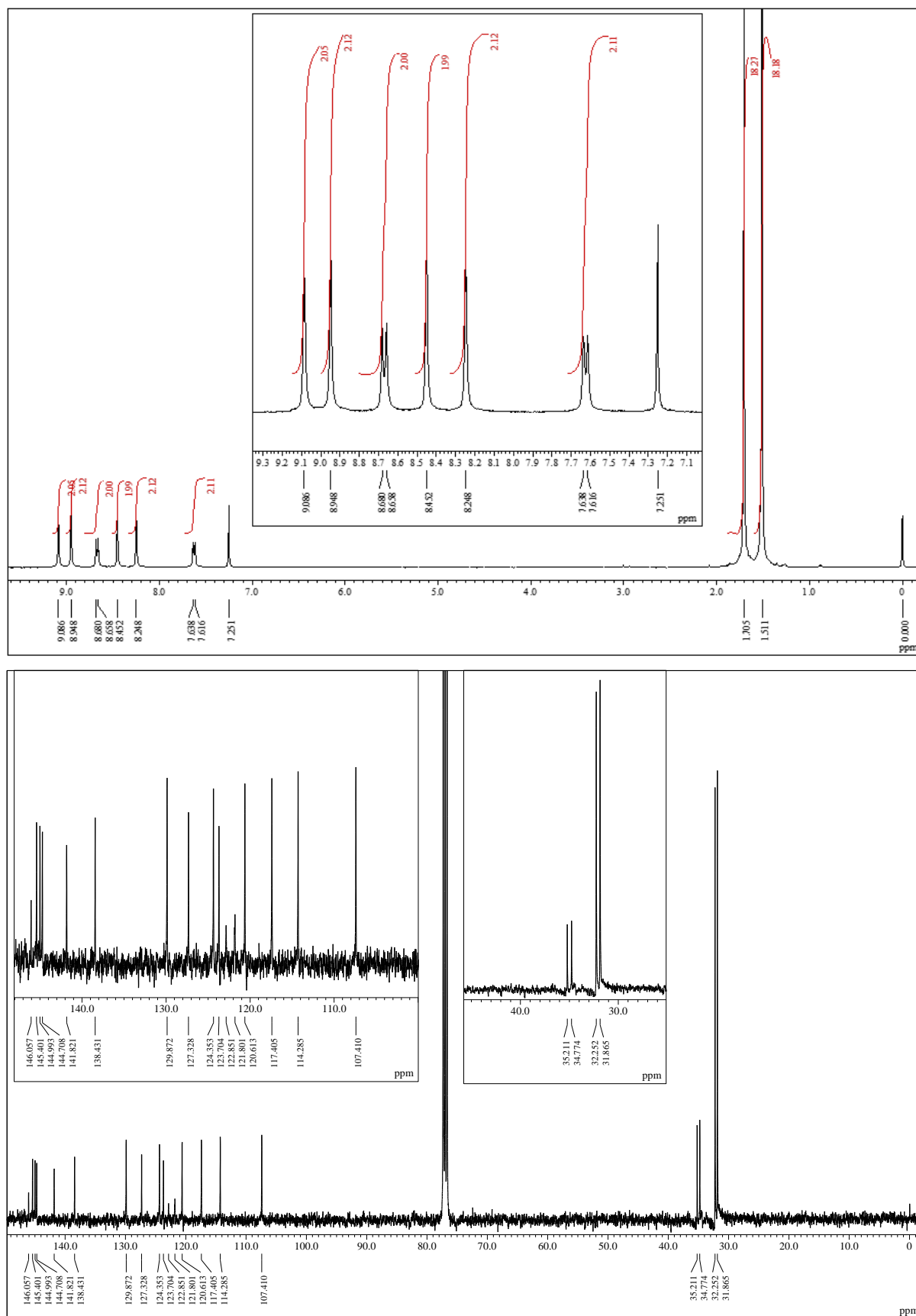


Fig. S1 ¹H and ¹³C NMR spectra of *p*-CzB in CDCl₃.

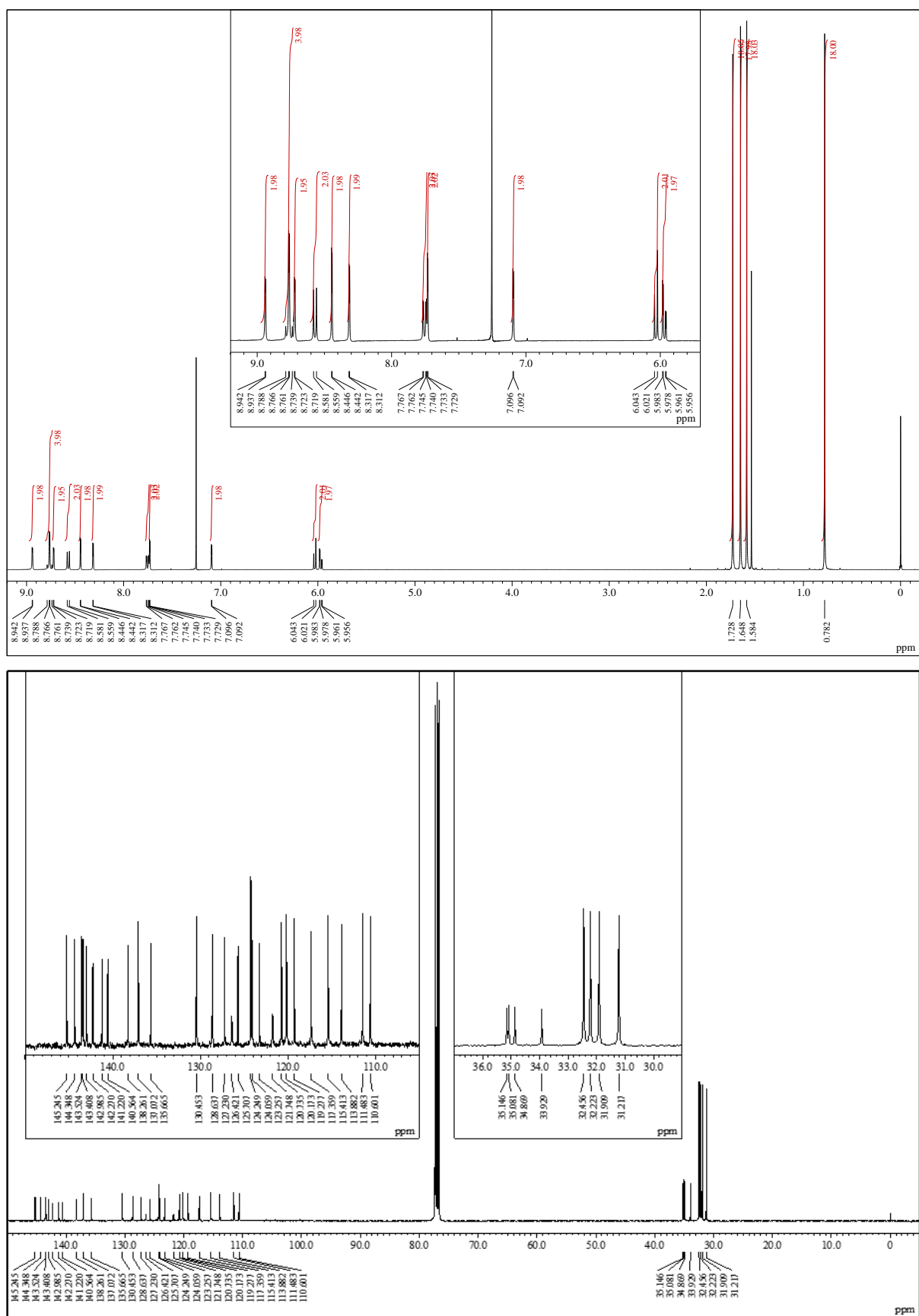


Fig. S2 ¹H and ¹³C NMR spectra of *m*-CzB in CDCl₃.

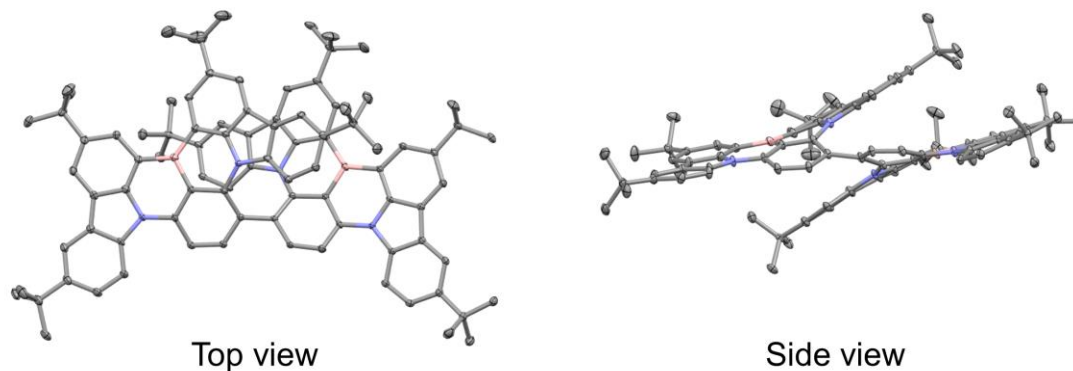


Fig. S3 X-ray structure of *m*-CzB with thermal ellipsoids at a 50% probability. Hydrogen atoms are omitted for clarity.

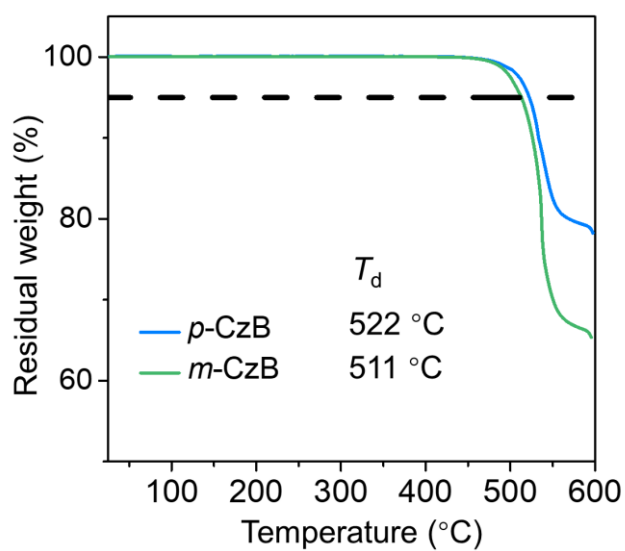


Fig. S4 TGA thermograms of *p*-CzB and *m*-CzB recorded at a heating rate of 10 °C min⁻¹ under N₂ (T_d = 5% weight-loss decomposition temperature).

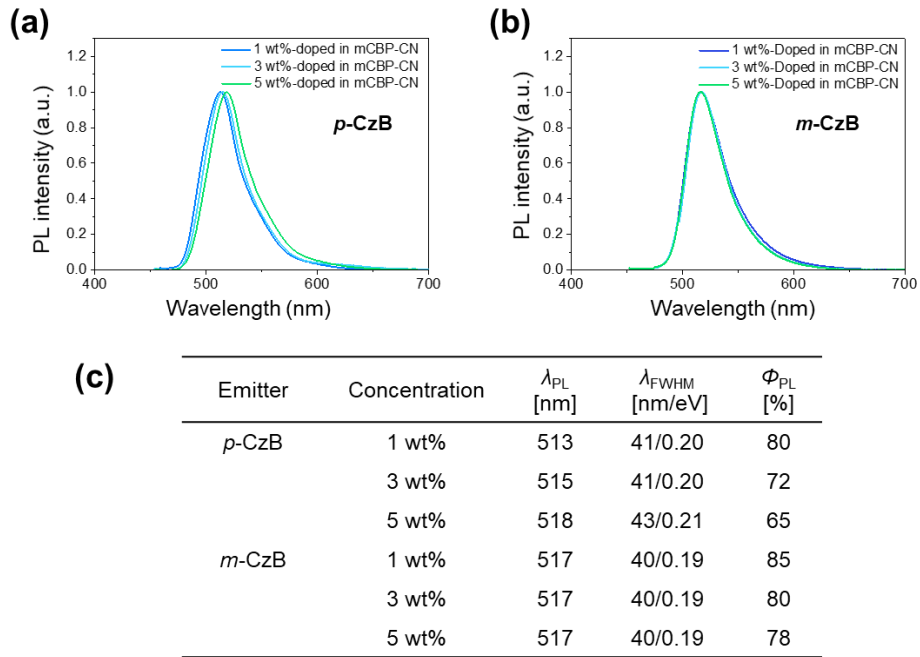


Fig. S5 Doping concentration dependence of PL spectra for (a) *p*-CzB and (b) *m*-CzB in mCBP-CN host matrices. (c) PL data of the doped films with different doping concentrations.

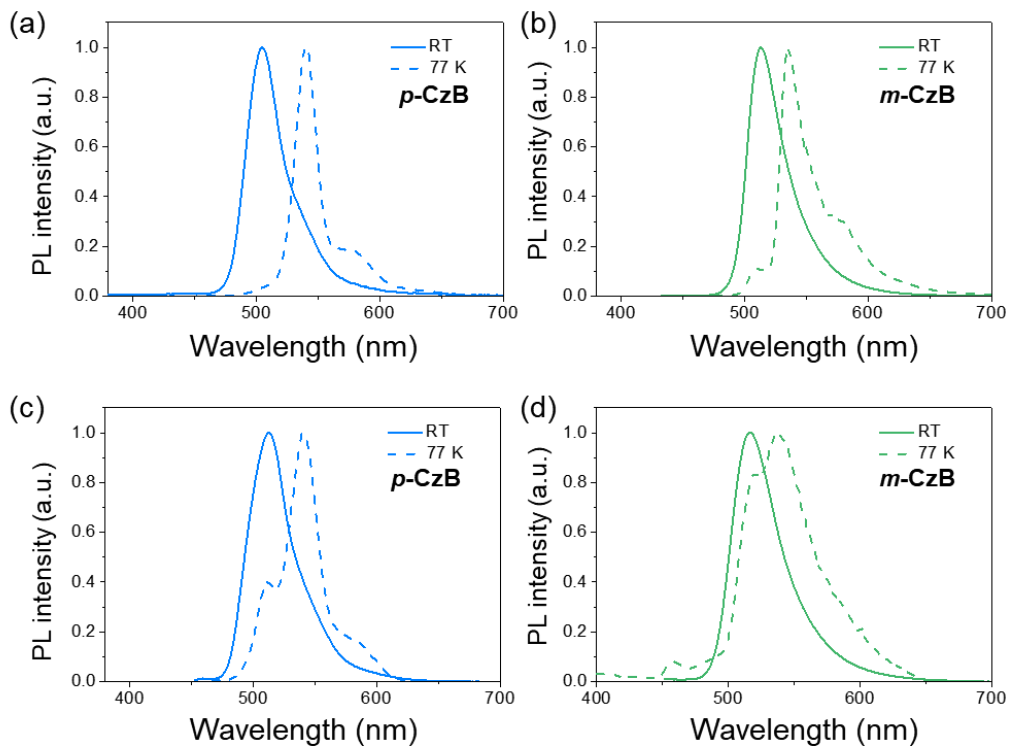


Fig. S6 Fluorescence (300 K) and phosphorescence (77 K) spectra of (a,c) *p*-CzB and (b,d) *m*-CzB in toluene solutions (10^{-5} M, top) and in the 1 wt%-doped films in mCBP-CN (bottom).

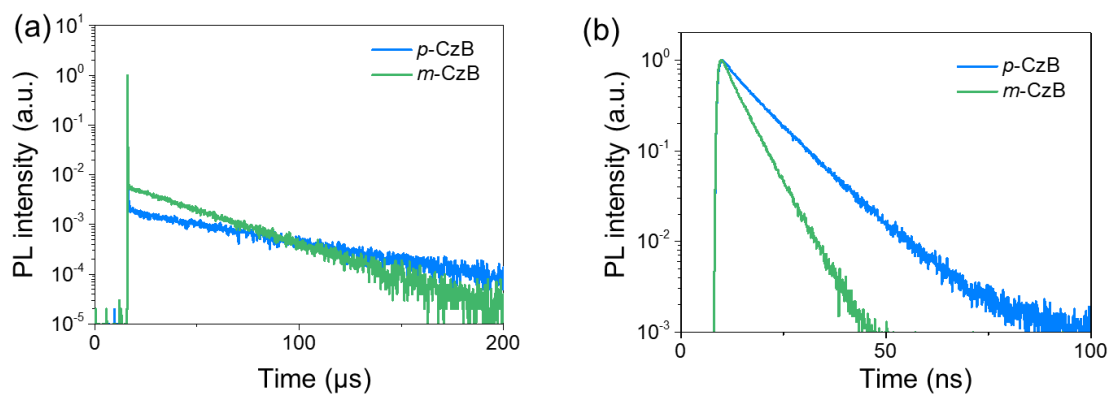


Fig. S7 Transient PL decay curves of *p*-CzB and *m*-CzB in deoxygenated toluene solutions (10^{-5} M) measured at 300 K in (a) 0–200 μ s and (b) 0–100 ns regions.

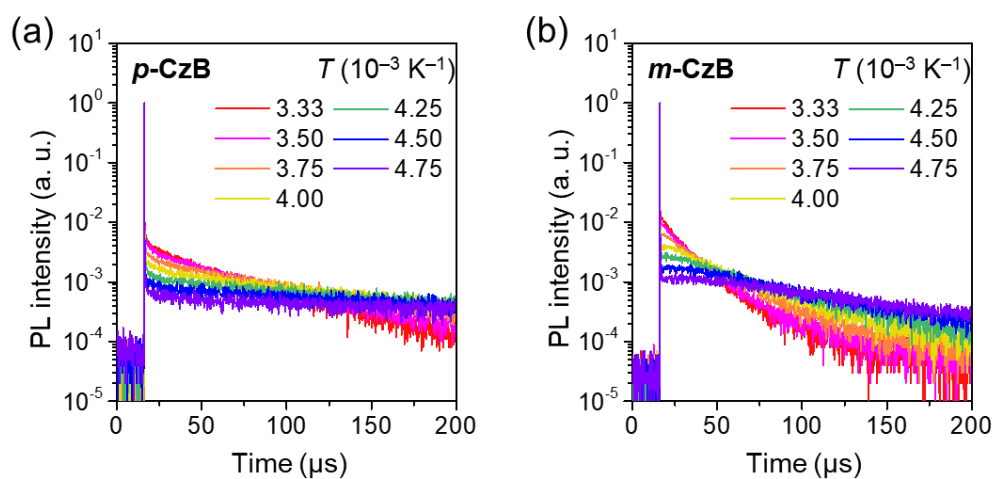


Fig. S8 Temperature dependence of transient PL decay curves for (a) *p*-CzB and (b) *m*-CzB in 1wt% doped films in mCBP-CN host.

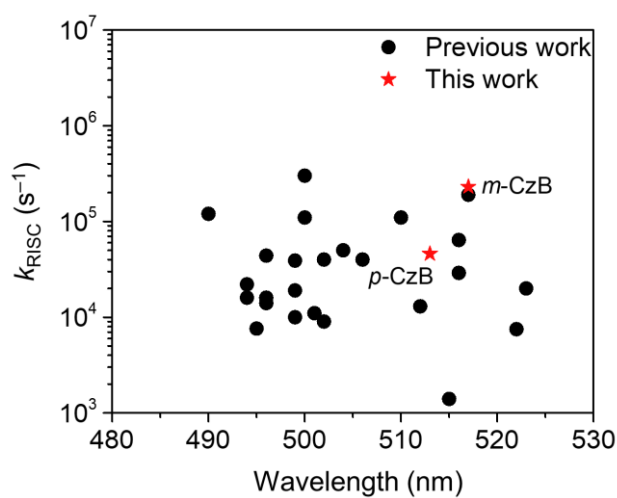


Fig. S9 Comparison of k_{RISC} values for the present and reported green MR-TADF emitters with CIE- $y \geq 0.50$.

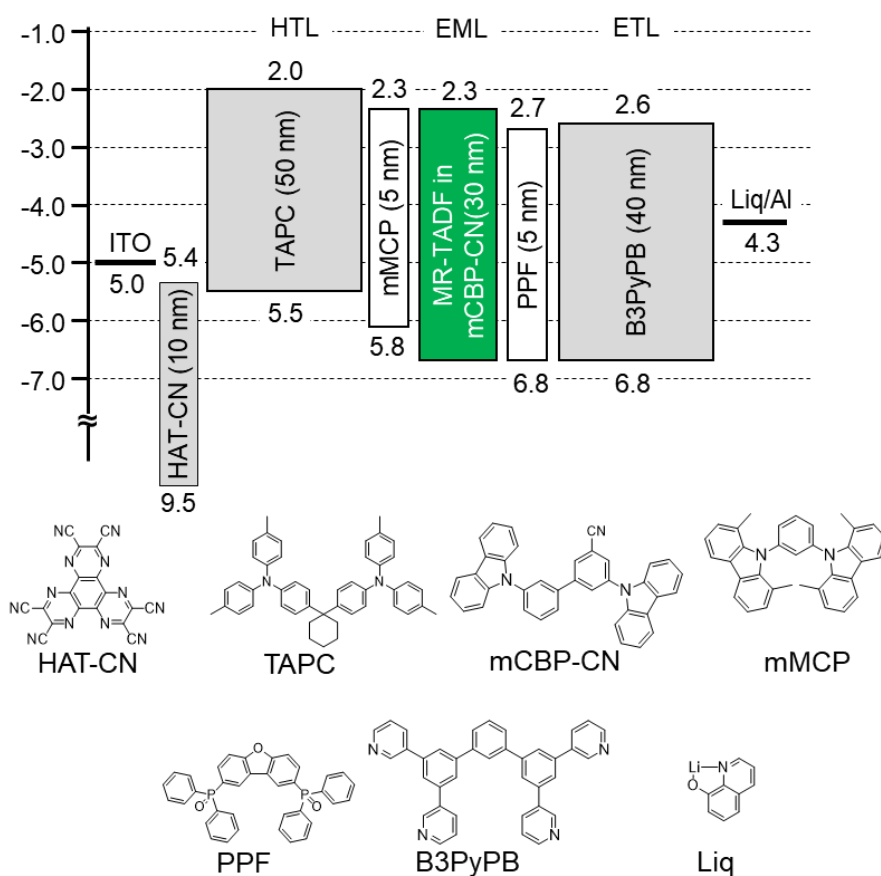


Fig. S10 Energy-level diagram and chemical structures of the materials used for TADF-OLEDs based on *p*-CzB and *m*-CzB.

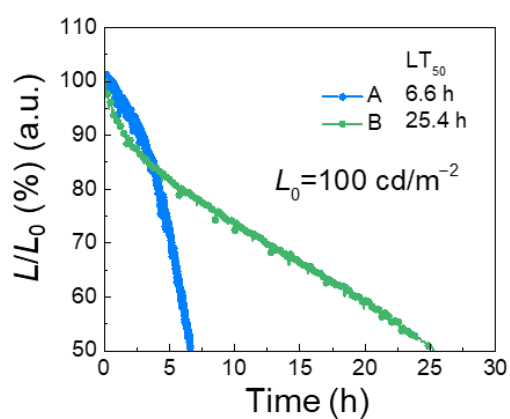


Fig. S11 Temporal changes of EL intensity for the TADF-OLEDs based on *p*-CzB and *m*-CzB with initial luminance at 100 cd m^{-2} .

Table S1. PL and EL data for green MR-TADF emitters

| emitter | λ_{PL} (nm) | Φ_{PL} (%) | τ_{d} (μs) | k_{RISC} (s^{-1}) | EQE_{max} (%) | EQE_{1000} (%) | roll-off (%) | CIE(x, y) | ref |
|---------------------|-------------------------------|---------------------------|----------------------------------------|------------------------------------------|----------------------------------|----------------------------|-----------------|------------|-----------|
| <i>p</i>-CzB | 513 | 80 | 41 | 4.6×10^4 | 20.2 | 9.3 | 54 | 0.16, 0.66 | this work |
| <i>m</i>-CzB | 517 | 85 | 15 | 2.3×10^5 | 23.5 | 15.0 | 36 | 0.20, 0.70 | this work |
| 2F-BN | 494 | 89 | 26 | 2.2×10^4 | 22.0 | 15.0 | 32 | 0.16, 0.60 | [S9] |
| 3F-BN | 499 | 83 | 17 | 3.9×10^4 | 22.7 | 21.1 | 7 | 0.20, 0.58 | [S9] |
| 4F-BN | 496 | 91 | 19 | 4.4×10^4 | 20.9 | 16.4 | 22 | 0.12, 0.48 | [S9] |
| AZA-BN | 522 | 94 | 164 | 7.5×10^3 | 25.7 | 9.0 | 64 | 0.27, 0.69 | [S10] |
| DtBuPhCzB | 496 | 90 | 61 | - | 23.4 | 5.7 | 75 | 0.15, 0.61 | [S11] |
| m-Cz-BNCz | 519 | 97 | - | 7.5×10^6 | 31.4 | 17.5 | 44 | 0.23, 0.69 | [S12] |
| BN-CP1 | 496 | 93 | 79 | 1.6×10^4 | 40.0 | 18.5 | 47 | 0.09, 0.50 | [S13] |
| BN-CP2 | 496 | 91 | 83 | 1.4×10^4 | 36.4 | 19.2 | 47 | 0.10, 0.53 | [S13] |
| BBCz-G | 517 | 99 | 13 | 1.9×10^5 | 31.8 | - | - | 0.26, 0.68 | [S8] |
| TCz-B | 512 | 89 | 71 | 1.3×10^4 | 29.2 | 9.4 | 68 | 0.16, 0.71 | [S14] |
| DPTRZ | 521 | 87 | 787 | 1.0×10^3 | 24.6 | 4.7 | 81 | 0.27, 0.60 | [S15] |
| TPTRZ | 501 | 95 | 83 | 1.1×10^4 | 29.8 | 12.4 | 58 | 0.23, 0.68 | [S15] |
| PPm | 499 | 96 | 87 | 1.0×10^4 | 28.6 | 10.2 | 64 | 0.17, 0.67 | [S15] |
| CNPm | 515 | 87 | 524 | 1.4×10^3 | 25.0 | 5.7 | 77 | 0.36, 0.62 | [S15] |
| NBNP | 500 | 93 | 3.8 | 3.0×10^5 | 28.0 | 25.6 | 8.0 | 0.09, 0.41 | [S16] |
| BN-TP | 523 | 96 | 44 | 2.0×10^4 | 35.1 | 20.8 | 40 | 0.26, 0.70 | [S17] |
| Tph-BN | 495 | 94 | 62 | 7.6×10^3 | 27.8 | 10.7 | 46 | 0.10, 0.46 | [S18] |
| pCz-BN | 496 | 95 | 89 | 1.4×10^4 | 28.9 | 15.6 | 55 | 0.13, 0.54 | [S18] |
| mCz-BN | 494 | 88 | 95 | 1.6×10^4 | 25.9 | 14.0 | 46 | 0.15, 0.55 | [S18] |
| BN1 | 499 | 93 | 69 | 1.9×10^4 | 17.0 | 8.5 | 50 | 0.15, 0.63 | [S19] |
| BN2 | 538 | 89 | 107 | 1.5×10^5 | 20.7 | 3.3 | 84 | 0.38, 0.61 | [S19] |
| BN-ICz-1 | 516 | 99 | 342 | 2.9×10^4 | 24.1 | 10.6 | 54 | 0.23, 0.72 | [S20] |
| BN-ICz-2 | 516 | 98 | 48.6 | 6.4×10^4 | 22.2 | 14.4 | 35 | 0.24, 0.73 | [S20] |
| OAB-ABP-1 | 506 | 90 | 32 | 4.0×10^4 | - | - | - | | [S21] |
| PXZBN | 502 | 90 | 91 | 0.9×10^4 | 23.3 | 11.5 | 51 | 0.22, 0.67 | [S22] |
| TPXZBN | 502 | 91 | 27 | 0.4×10^5 | 21.3 | 17.4 | 18 | 0.16, 0.65 | [S23] |
| DPXCZBN | 500 | 90 | 15 | 1.1×10^5 | 19.2 | 17.2 | 11 | 0.15, 0.64 | [S23] |
| BN-DPAC | 490 | 86 | 11.6 | 1.2×10^5 | 23.5 | 16.3 | 31 | 0.14, 0.56 | [S24] |
| 2PXZBN | 504 | 78 | 25.3 | 0.5×10^5 | 17.1 | 7.4 | 58 | 0.28, 0.64 | [S25] |
| 2PTZBN | 510 | 58 | 16.1 | 1.1×10^5 | 25.1 | 17.2 | 33 | 0.28, 0.65 | [S25] |

References

- [S1] Park, I. S.; Min, H.; Kim, J. U.; Yasuda, T. *Adv. Optical Mater.* **2021**, *9*, 2101282.
- [S2] Ihn, S.-G.; Lee, N.; Jeon, S. O.; Sim, M.; Kang, H.; Jung, Y.; Huh, D. H.; Son, Y. K.; Lee, S. Y.; Numata, M.; Miyazaki, H.; Gómez-Bombarelli, R.; Aguilera-Iparraguirre, J.; Hirzel, T.; Aspuru-Guzik, A.; Kim, S.; Lee, S. *Adv. Sci.* **2017**, *4*, 1600502.
- [S3] Sasabe, H.; Gonmori, E.; Chiba, T.; Li, Y. J.; Tanaka, D.; Su, S. J.; Takeda, T.; Pu, Y. J.; Nakayama, K. I.; Kido, J. *Chem. Mater.* **2008**, *20*, 5951–5953.
- [S4] ADF2021, SCM, Theoretical Chemistry, Vrije Universiteit, Amsterdam, The Netherlands, <http://www.scm.com/>.
- [S5] Wang, F.; Ziegler, T. *J. Chem. Phys.* **2005**, *123*, 4211–4214.
- [S6] Y.-T. Li, E.; Jiang, T. -Y.; Chi, Y.; Chou, P. -T. *Phys. Chem. Chem. Phys.* **2014**, *16*, 26184–26192.
- [S7] Goushi, K.; Yoshida, K.; Sato, K.; Adachi, C. *Nat. Photonics* **2012**, *6*, 253–258.
- [S8] Yang, M.; Park, I. S.; Yasuda, T. *J. Am. Chem. Soc.* **2020**, *142*, 19468–19472.
- [S9] Zhang, Y.; Zhang, D.; Wei, J.; Liu, Z.; Lu, Y.; Duan, L. *Angew. Chem. Int. Ed.* **2019**, *58*, 16912–16917.
- [S10] Zhang, Y.; Zhang, D.; Wei, J.; Hong, X.; Lu, Y.; Hu, D.; Li, G.; Liu, Z.; Chen, Y.; Duan, L. *Angew. Chem. Int. Ed.* **2020**, *59*, 17499–17503.
- [S11] Xu, Y.; Cheng, Z.; Li, Z.; Liang, B.; Wang, J.; Wei, J.; Zhang, Z.; Wang, Y. *Adv. Optical Mater.* **2020**, *8*, 1902142.
- [S12] Xu, Y.; Li, C.; Li, Z.; Wang, Q.; Cai, X.; Wei, J.; Wang, Y. *Angew. Chem. Int. Ed.* **2020**, *59*, 17442–17446.
- [S13] Jiang, P.; Miao, J.; Cao, X.; Xia, H.; Pan, K.; Hua, T.; Lv, X.; Huang, Z.; Zou, Y.; Yang, C. *Adv. Mater.* **2022**, *34*, 2106954.
- [S14] Yang, M.; Shikita, S.; Min, H.; Park, I. S.; Shibata, H.; Amanokura, N.; Yasuda, T. *Angew. Chem. Int. Ed.* **2021**, *60*, 23142–23147.
- [S15] Xu, Y.; Li, C.; Li, Z.; Wang, J.; Xue, J.; Wang, Q.; Cai, X.; Wang, Y. *CCS Chem.* **2022**, *4*, 2065–2079.
- [S16] Luo, X. F.; Ni, H. X.; Ma, H. L.; Qu, Z. Z.; Wang, J.; Zheng, Y. X.; Zuo, J. L. *Adv. Optical Mater.* **2022**, *10*, 2102513.
- [S17] Xu, Y.; Wang, Q.; Wei, J.; Peng, X.; Xue, J.; Wang, Z.; Su, S.-J.; Wang, Y. *Angew. Chem. Int. Ed.* **2022**, *61*, e202204652.
- [S18] Liu, F.; Cheng, Z.; Wan, L.; Feng, Z.; Liu, H.; Jin, H.; Gao, L.; Lu, P.; Yang, W. *Small* **2022**, *18*, 2106462.
- [S19] Wu, X.; Huang, J.; Su, B.; Wang, S.; Yuan, L.; Zheng, W.; Zhang, H.; Zheng, Y.; Zhu, W.; Chou, P. *Adv. Mater.* **2022**, *34*, 2105080.
- [S20] Zhang, Y.; Li, G.; Wang, L.; Huang, T.; Wei, J.; Meng, G.; Wang, X.; Zeng, X.; Zhang, D.; Duan, L. *Angew. Chem. Int. Ed.* **2022**, *61*, e202202380.

- [S21] Ikeda, N.; Oda, S.; Matsumoto, R.; Yoshioka, M.; Fukushima, D.; Yoshiura, K.; Yasuda, N.; Hatakeyama, T. *Adv. Mater.* **2020**, *32*, 2004072.
- [S22] Liu, G.; Sasabe, H.; Kumada, K.; Matsunaga, A.; Katagiri, H.; Kido, J. *Mater. Chem. C* **2021**, *9*, 8308–8313.
- [S23] Hu, J. J.; Luo, X. F.; Zhang, Y. P.; Mao, M. X.; Ni, H. X.; Liang, X.; Zheng, Y. X. *J. Mater. Chem. C* **2022**, *10*, 768–773.
- [S24] Jiang, P.; Zhan, L.; Cao, X.; Lv, X.; Gong, S.; Chen, Z.; Zhou, C.; Huang, Z.; Ni, F.; Zou, Y.; Yang, C. *Adv. Opt. Mater.* **2021**, *9*, 2100825.
- [S25] Hua, T.; Zhan, L.; Li, N.; Huang, Z.; Cao, X.; Xiao, Z.; Gong, S.; Zhou, C.; Zhong, C.; Yang, C. *Chem. Eng. J.* **2021**, *426*, 131169.